MOLECULAR AND CELLULAR BIOLOGY, May 1996, p. 2065–2073 Vol. 16, No. 5
0270-7306/96/$04.00+0

Characterization of the Cooperative Function of Inhibitory Sequences in Ets-1

MATTHEW D. JONSEN, JEANNINE M. PETERSEN, QING-PING XU, AND BARBARA J. GRAVES*

Department of Oncological Sciences, Division of Molecular Biology and Genetics, Huntsman Cancer Institute, University of Utah School of Medicine, Salt Lake City, Utah 84132

Received 8 December 1995/Returned for modification 18 January 1996/Accepted 9 February 1996

DNA binding by the eukaryotic transcription factor Ets-1 is negatively regulated by an intramolecular mechanism. Quantitative binding assays compared the DNA-binding activities of native Ets-1, three deletion mutants, and three tryptic fragments. Ets-1 and activated Ets-1 polypeptides differed in DNA-binding affinity as much as 23-fold. Inhibition was mediated by two regions flanking the minimal DNA-binding domain. Both regions regulated affinity by enhancing dissociation of the protein-DNA complex. Three lines of evidence indicated that inhibition requires cooperative interaction between the two regions: first, the two inhibitory regions acted through a common mechanism; second, neither region functioned independently of the other; finally, mutation of the C-terminal inhibitory region altered the conformation of the N-terminal inhibitory region. In addition, partial proteolysis detected an identical altered conformation in the N-terminal inhibitory region of Ets-1 bound to DNA. This finding suggested that repression is transiently disrupted during DNA binding. These results provide evidence that the two inhibitory regions of Ets-1 are structurally, as well as functionally, coupled. In addition, conformational change is shown to be a critical component of the inhibition mechanism. A cooperative, allosteric model of autoinhibition is described. Autoinhibition of Ets-1 could be relieved by either protein partner(s) or posttranslational modifications.

Transcription factors are modular proteins with domains for DNA binding, subunit association, and transcriptional activation. The relative independence of these functional domains leads to the picture of transcription factors as composite molecules with discrete, autonomous units (11). The phenomenon of intramolecular inhibition expands this view. In many cases, functional domains are modulated by other regions of the protein. For example, trimerization of *Drosophila* heat shock factor is regulated by inhibitory sequences (40), and the activation domains of CRP2 (C/EBPβ) (28, 52) and mammalian heat shock factor (18, 42, 55) are negatively modulated by flanking regions. In the case of NF-κB, an N-terminal region of the p105 subunit inhibits DNA binding, and repression is relieved in vivo by proteolytic processing (19). Intramolecular inhibition of DNA binding also has been reported for p53 (25, 26) and TATA-binding protein (32). These examples demonstrate that intact proteins, in addition to minimal functional domains, must be analyzed to understand fully how transcription factors regulate gene expression.

DNA binding activity of the eukaryotic transcription factor Ets-1 is also negatively regulated by an intramolecular mechanism. The *ets* family of transcription factors is defined by a highly conserved DNA-binding module, termed the ETS domain. Recently, nuclear magnetic resonance (NMR) structural analyses have determined that the ETS domain displays a winged helix-turn-helix motif (4, 5, 31, 51). These structural studies demonstrate that the ETS domain is compact and well folded in the presence and absence of DNA. Nevertheless, this minimal DNA-binding domain is modulated by the remainder of the protein. Studies of deletion mutants and natural variants of Ets-1 indicate that flanking sequences negatively regulate the ETS domain. In several cases, N-terminal deletion mutants display higher binding activity than the full-length protein (22, 33, 36, 49). Alternative splicing of *ets-1* mRNA, which removes 342 bp of internal coding sequence, also results in a protein product with DNA-binding activity higher than that of full-length Ets-1 (8, 49). Deletion of residues C-terminal to the ETS domain also increases the binding activity (22, 23, 33). This latter deletion mimics one of the alterations in the *ets-1* gene transduced by the retrovirus E26 (30, 35). These studies led to a model of two inhibitory regions working together to sterically mask the DNA-binding surface (33).

This report extends previous studies of Ets-1 intramolecular inhibition in four important ways. First, quantitative DNA binding studies of full-length Ets-1 as well as N- and C-terminal truncations provided strong evidence that the two inhibitory regions function cooperatively. Second, kinetic experiments demonstrated that the two inhibitory regions decrease DNA binding by destabilizing protein-DNA complexes, not by masking the DNA-binding surface. Third, partial proteolysis indicated that the two inhibitory regions are structurally coupled within the full-length protein. Fourth, proteolysis experiments detected a structural rearrangement in Ets-1 bound to DNA, as well as in a high-affinity DNA-binding species. These findings led to a new mechanistic model of inhibition that includes the following features: (i) inhibition is mediated by coupling of the two inhibitory regions, (ii) intramolecular interactions between the inhibitory regions destabilize protein-DNA complexes by an allosteric mechanism, and (iii) uncoupling of the two inhibitory regions leads to a conformational change in the inhibitory regions and altered binding properties of the ETS domain. Thus, conformational change and intramolecular interactions are critical to the mechanism of autoinhibition.

MATERIALS AND METHODS

Protein expression and purification. The Ets-1 polypeptides were expressed in *Escherichia coli* BL21(DE3):pLysS with the pET vector system and mouse *ets-1* cDNA. For full-length Ets-1, the expression vector pET-ets-1 was used (36). Bacterial cultures grown in rich medium were induced at mid-log phase for 3 h with 1 mM isopropyl-β-D-thiogalactopyranoside. For purification, bacterial pel-

* Corresponding author. Phone: (801) 581-7308. Fax: (801) 581-3607. Electronic mail address: Graves@bioscience.utah.edu.

lets were lysed by two freeze-thaw cycles and then resuspended in 25 ml of TNU (10 mM Tris-Cl [pH 7.6 at 25°C], 150 mM NaCl, 5 M urea) with 0.1% Triton X-100 per liter of culture. Lysed bacterial suspension was sonified at 4°C for 4 min (50% output; Heat Systems, Inc.). The lysate was then passed over a DEAE-Sepharose (Pierce) column equilibrated in TNU. The unbound protein fraction was dialyzed against TEK_{50} (25 mM Tris-Cl [pH 7.9], 0.1 mM EDTA, 50 mM KCl; the subscript refers to millimolar concentration of KCl) with 10% glycerol, 1 mM dithiothreitol (DTT), and 1 mM phenylmethylsulfonyl fluoride. Dialysates were centrifuged at 85,000 × *g* for 30 min at 4°C, passed through a 0.2-μm-pore-size syringe filter, and applied to a 22-ml S-Sepharose column (Pharmacia) equilibrated in TEK_{50} with 10% glycerol. Bound proteins were eluted with a linear KCl gradient (50 to 1,000 mM) developed over 10 column volumes. Ets-1 eluted between 100 and 200 mM KCl.

Details of vector construction, expression, and purification for ΔN331 are described elsewhere (37). In brief, the open reading frame contains a methionine codon linked to the native murine *ets-1* codons 331 to 440. The truncated polypeptide was expressed in bacteria, and soluble protein was purified by DEAE-cellulose and S-Sepharose chromatography.

The concentration of total protein for ΔN331 and Ets-1 was measured spectrophotometrically, using molar extinction coefficients that were determined experimentally (15) (for Ets-1, 7.1×10^4 M^{-1} cm^{-1} at 278 nm; for ΔN331, 3.2×10^4 M^{-1} cm^{-1} at 280 nm). The concentration of active protein was assayed in DNA titration experiments (see below). Purity, as judged by densitometry of Coomassie blue-stained sodium dodecyl sulfate (SDS)-polyacrylamide gels, was greater than 90% for ΔN331 and Ets-1.

The expression vector for the C-terminal deletion mutant ΔC428 was engineered in three steps. A 378-bp DNA fragment containing codons 310 through 428 of the mouse *ets-1* cDNA was generated by PCR, subcloned into pKS Bluescript vector (Stratagene), and sequenced. The design of the PCR primers placed an *Nde*I site at the 5′ end of the fragment and a stop codon and *Bam*HI restriction site at the 3′ end. A 198-bp *Hin*dIII-*Bam*HI fragment that contained codons 388 to 428 was then isolated from the subclone and used to replace codons 388 to 440 of *ets-1* cDNA in pET-ets-1. Finally, the engineered cDNA with codons 1 to 428 was placed into pAED (3). Expression in bacteria and purification were performed as described for Ets-1. ΔC428 eluted from the S-Sepharose between 150 and 250 mM KCl. Active fractions were pooled, dialyzed against TEK_{50} with 10% glycerol, and then loaded onto a 1-ml Mono Q (Pharmacia) column. ΔC428 eluted between 200 and 300 mM KCl within a linear elution gradient of KCl (50 to 1,000 mM). The concentration of total protein was measured spectrophotometrically, using the molar extinction coefficient 7.9×10^4 M^{-1} cm^{-1} at 280 nm. The purity was approximately 90% as determined by densitometry of Coomassie blue-stained SDS-polyacrylamide gels. Two non-DNA-binding contaminants contributed to absorbance. The concentration of active protein was determined in DNA titration experiments (see below).

ED(331-415) contains a methionine codon linked to the native murine Ets-1 residues 331 to 415 (37). The truncated polypeptide was expressed in bacteria, and soluble protein was partially purified by DEAE-cellulose and S-Sepharose chromatography to 50% purity. The concentration of ED(331-415) was estimated from Coomassie blue-stained gels, using ΔN331 as a standard.

Oligomeric binding site DNA. All DNA binding assays were performed with oligomeric DNA containing the high-affinity Ets-1 binding site SC1 (36). Complementary oligonucleotides contained the sequence 5′-CGGCCAAGCCGGAA GTGAGTGCC-3′ in duplex and overhanging 5′ ends of the sequence 5′-TCG A-3′. Oligonucleotides were purified on an 18% acrylamide–urea gel electrophoresed in 1× TBE buffer (90 mM Tris-borate [pH 8.3], 2 mM EDTA) and then subjected to reverse-phase chromatography on Sep-Pak columns (Millipore) and gel filtration on BioSpin 6 columns (Bio-Rad). Oligonucleotide concentrations were obtained by A_{260}, using calculated extinction coefficients (top, 2.59×10^5 M^{-1} cm^{-1}; bottom, 2.39×10^5 M^{-1} cm^{-1}) determined by Oligo (version 4.0; National Biosciences, Inc.). Single-stranded oligonucleotides were radiolabeled with [γ-^{32}P]ATP and T4 polynucleotide kinase and then fractionated from unincorporated [γ-^{32}P]ATP by gel filtration on BioSpin 6 columns. Duplex DNA was obtained by mixing complementary oligonucleotides at a 1:1 molar ratio, boiling in TEK_{60} for 3 min, and cooling to room temperature over 2 h.

Gel mobility shift assay. For mobility shift assays, DNA binding reactions and electrophoresis were performed as previously described (36). Following electrophoresis, the gels were dried and exposed to either PhosphorImager screens (Molecular Dynamics) or preflashed X-ray film (Cronex; Dupont) in the presence of an intensifying screen. Radioactivity was quantified by using volume integration of individual bands on phosphor images.

Quantitative analyses of DNA binding. To determine the concentration of active protein, reaction mixtures contained known concentrations of radiolabeled SC1 duplex DNA ($[D_t]$; at indicated concentrations) and a fixed amount of protein ($[P_t]$). The experiment was designed to measure the fraction of free DNA, $[D]/[D_t]$, which is the parameter most accurately measured in a mobility shift assay (1). For each concentration of total DNA, $[D_t]$, two reaction mixtures, an experimental (with protein) and a control (without protein), were assayed. First, $[D]/[D_t]$ was determined by dividing the free DNA signal in the experimental lane by the free DNA signal in the control lane. The fraction of DNA in complex was then calculated from the equation $[PD]/[D_t] = 1 - ([D]/[D_t])$. The concentration of protein bound at each DNA concentration $[PD] = ([PD]/[D_t])[D_t]$, was then calculated. For graphing, the fraction of protein active was calculated by dividing $[PD]$ by the concentration of total input protein, $[P_t]$, as determined from extinction coefficients.

To determine equilibrium dissociation constants (K_Ds), various concentrations of Ets-1 polypeptides were incubated with a fixed amount of radiolabeled SC1 duplex DNA. Free and bound DNA fractions were resolved by mobility shift assay. The DNA concentration was kept at least 10 times lower than the estimated K_D value, ensuring that $[P_t]$ was an accurate estimate of free protein $[P]$. $[D]/[D_t]$ was the ratio of the free DNA signal at each protein concentration to the free DNA signal in a control lane containing no protein. The fraction of DNA in complex, $[PD]/[D_t]$, is equal to $1 - ([D]/[D_t])$. All datum points were fitted to the rearranged mass action equation $[PD]/[D_t] = 1/(1 + \{K_D/[P_t]\})$ by using nonlinear least-squares analyses (Kaleidagraph; Synergy Software). The deviation of the data from the curve fit at the higher protein concentrations could be explained by either a fraction of the DNA being inactive or a portion of complexes dissociating during gel entry.

To determine dissociation rate constants, k_{-1}, protein and radiolabeled SC1 duplex DNA (8.5×10^{-10} M) were incubated under standard conditions. The active protein concentration was 5×10^{-9} M except in the case of renatured tryptic fragments and ED(331-415), for which no concentration estimate was obtained. Note that these kinetic experiments do not require an accurate concentration of active protein since only disassociation of active complexes is monitored. After at least a 15-min incubation period, one control aliquot was removed and mixed with 1/10 volume of TEK_{60}. To the remaining reaction mixture, a 1,000-fold excess unlabeled SC1 DNA in 1/10 volume of TEK_{60} was added. Following a brief vortexing (which allowed immediate mixing and in controls showed no effect on binding activity), aliquots were removed at intervals and immediately loaded on a running mobility shift gel. The ratio of the shifted signal at each time point to the signal in the control lane was presented as $[PD_t]/[PD_0]$, the fraction of original complex remaining at time *t*. The dissociation rate constant, k_{-1}, was determined by least-squares analyses (Kaleidagraph; Synergy Software) of the equation $\ln[PD_t]/[PD_0] = -k_{-1}\,t$.

Protease studies. Lyophilized trypsin (Sigma catalog no. T8642) was resuspended in 25 mM Tris-Cl (pH 7.6)–10 mM $CaCl_2$ at 4°C. Protease was added to 10 μg of Ets-1 polypeptides in TEK_{50} with 10% glycerol and 1 mM DTT at a ratio of 1:10 (enzyme/protein, vol/vol), with final concentrations as given in the figure legends. Digestion proceeded at room temperature for 2 min and was stopped by addition of 3× loading buffer (1.5% SDS, 7.5% glycerol, 0.0075% bromophenol blue, 0.2 M Tris-Cl [pH 6.8], 50 mM DTT [freshly prepared]) and immediate boiling at 95°C for 5 min. Proteolytic fragments were fractionated on SDS–10 to 22% linear gradient polyacrylamide gels (29) and visualized by staining with Coomassie blue. For digestion in the presence of DNA, 10 μg of Ets-1 or ΔC428 was incubated with ~5 μM duplex SC1 DNA for 20 min under standard binding conditions prior to digestion. This concentration of DNA is sufficient to achieve >95% protein occupancy.

For kinetic experiments on tryptic fragments, tryptic fragment T3, T4, or T5 was renatured from a 10 to 22% polyacrylamide–SDS gel (21). In brief, gel slices were crushed and soaked in elution buffer (0.1% SDS, 50 mM Tris [pH 7.9], 150 mM KCl, 0.1 mM EDTA, 0.1 mg of bovine serum albumin [BSA] per ml, 5 mM DTT) at room temperature for 12 h. Gel fragments were removed by filtering the supernatant through cellulose acetate (Schleicher & Schuell), and then proteins were precipitated with acetone, dried, and resuspended in 6 M guanidine-HCl in dilution buffer (50 mM Tris-HCl [pH 7.9], 20% glycerol, 150 mM KCl, 1 mM DTT, 0.1 mM EDTA, 0.18 mg of BSA per ml). Proteins were renatured by 20-fold dilution in TEK_{50} with 10% glycerol, 0.2 mg of BSA per ml, and 1 mM DTT at 4°C for 30 min. No estimate of Ets-1 polypeptide concentration or fraction of molecules active was obtained.

Western blot (immunoblot) analysis was performed by standard procedures (24). Primary antibodies, which were specific for the 11 amino acids at the C terminus of Ets-1 (20), had been affinity purified and were added directly to the blocking buffer at a dilution of 1:2,500. After an overnight incubation at 4°C, alkaline phosphatase-conjugated secondary antibody was used for visualization of antigen-antibody complexes.

For N-terminal sequencing, tryptic fragments were separated on gradient SDS-polyacrylamide gels, transferred to polyvinylidene difluoride membranes in 3-[cyclohexylamino]-1-propanesulfonic acid (CAPS) buffer (pH 11), and visualized by Coomassie blue staining. After extensive washing in deionized H_2O, Edman sequencing was performed directly on the membrane with an automated sequencer (model 477A; Applied Biosystems, Inc.).

RESULTS

Two inhibitory regions modulate Ets-1 DNA binding. Two regions of Ets-1 that lie on either side of the ETS domain have been reported to affect DNA binding. To further investigate this autoinhibition, we compared DNA-binding characteristics of Ets-1 and two deleted species, ΔN331, an N-terminal deletion, and ΔC428, a C-terminal deletion (Fig. 1A). Proteins were expressed in bacteria and purified, and then DNA-binding activity was analyzed by quantitative mobility shift assays.

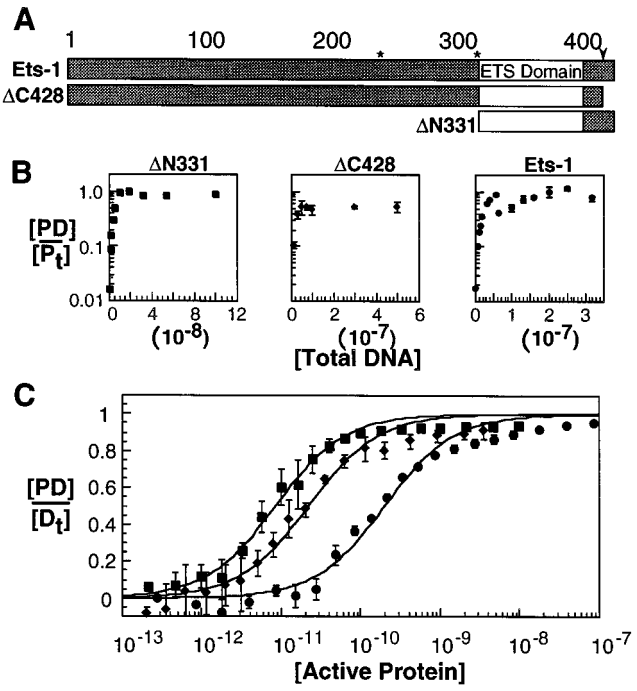

FIG. 1. Equilibrium DNA-binding studies of Ets-1 and deletion mutants ΔC428 and ΔN331 demonstrate a difference in affinity. Data were obtained from mobility shift assays and analyzed as described in Materials and Methods. (A) Schematic representation of full-length Ets-1 (residues 1 to 440), the C-terminal deletion polypeptide, ΔC428, and the N-terminal deletion polypeptide, ΔN331. The ETS domain (open bar) corresponds to the highly conserved region (residues 331 to 415) present in all *ets* family members. Asterisks mark the boundaries of exon VII, and the arrowhead indicates the last *ets-1* codon transduced by the E26 retrovirus. (B) Determination of active protein concentration of ΔN331, ΔC428, and Ets-1. The fraction ($\log_{10}$) of total protein bound to DNA, $[PD]/[P_t]$, is presented as the mean (± standard deviation) of two or three independent experiments. (C) Determination of K_D. Mobility shift assays were performed with active ΔN331 (squares), ΔC428 (diamonds), or Ets-1 (circles) at the indicated concentrations and a $[D_t]$ of less than 8×10^{-13} M. $[PD]/[D_t]$ is presented as the mean (± standard deviation) of two or three independent experiments. Data were fitted to the equation $[PD]/[D_t] = 1/(1 + \{K_D/[P]\})$ by using nonlinear least squares.

DNA titration experiments were performed to determine the concentration of protein capable of binding DNA (Fig. 1B). Active protein concentrations were then used in protein titrations to determine the K_D for a high-affinity binding site, SC1 (36). The DNA-binding affinity of full-length Ets-1 was lower than those of the N- and C-truncated versions by 23- and 9-fold, respectively (Fig. 1C; Table 1). These studies establish that removal of either region increases DNA-binding affinity to a similar level. In addition, the independent determination of active protein concentrations demonstrated that the lower affinity of full-length Ets-1 is not due to a difference in protein activity. These two quantitative experiments are also consistent with previous reports that Ets-1 binds the high-affinity binding site SC1 as a monomer (36).

TABLE 1. DNA-binding properties of full-length and truncated Ets-1

Protein	Mean K_D (pM) ± SD	k_{-1} (s^{-1})	$t_{1/2}$[a]	k_1 (M^{-1} s^{-1}, 10^8)[b]
Ets-1	200 ± 20	≥0.12	≤5.8	≥6
ΔN331	8.5 ± 0.7	0.012	58	14
ΔC428	22 ± 2	0.016	43	7
ED(331-415)	ND[c]	0.016	43	

[a] Calculated from the equation $t_{1/2} = 0.693/k_{-1}$.
[b] Calculated from the equation, $k_1 = k_{-1}/K_D$.
[c] ND, assay not done.

We next investigated the molecular basis for the difference in affinity by measuring the dissociation rates of protein-DNA complexes in quantitative mobility shift assays. Binding reaction mixtures, containing radiolabeled SC1 duplex DNA and Ets-1 proteins, were allowed to reach equilibrium, and then, a 1,000-fold molar excess of unlabeled SC1 duplex DNA was added. At timed intervals, aliquots were loaded onto a mobility shift gel to monitor decay of the radiolabeled complex (Fig. 2A). The half-life of each protein-DNA complex was determined by an exponential decay plot (Fig. 2C). The time axis was adjusted by 15 s to account for the expected time delay between mixing and entry of molecules into the gel matrix (1, 12). The dissociation rate constants were very similar for ΔN331-DNA and ΔC428-DNA complexes, corresponding to half-lives of 58 and 43 s, respectively (Fig. 2A and C; Table 1). In contrast, a maximal estimate of the half-life of the Ets-1–DNA complex was only ~6 s. These results demonstrate that the dissociation rate constants of the high-affinity complexes differ from that of the low-affinity Ets-1–DNA complex by at least sevenfold. Thus, the majority of the difference in binding affinities of Ets-1 species was due to the dissimilarity in dissociation rates (Table 1). These findings indicate that both N- and C-terminal inhibitory regions negatively regulate DNA binding by enhancement of dissociation. Furthermore, the similarity in the levels of activation upon removal of either inhibitory region, as measured by dissociation experiments, suggests that these inhibitory regions act through a common pathway.

Equilibrium and kinetic binding studies indicated that both inhibitory regions are required to mediate inhibition. Neither region alone effectively represses the DNA-binding activity of the ETS domain. Specifically, ΔN331 contains an intact C-terminal inhibitory region yet displays high affinity. Likewise, ΔC428 contains an intact N-terminal inhibitory region and also displays high affinity. We performed a final test for cooperativity between the two regions by construction of a mutant, ED(331-415), that lacks both inhibitory regions. Dissociation measurements demonstrated that this minimal DNA-binding polypeptide had a half-life of 43 s and, therefore, the same slow dissociation rate displayed by the N- and C-terminal deletion mutants (Fig. 2B and C; Table 1). Thus, removal of both inhibitory regions did not increase the level of activation above that displayed by either of the singly deleted species. This result provided final evidence that the two regions mediate inhibition through a common pathway.

Partial proteolysis of Ets-1 implicates structural coupling of inhibitory regions. Functional cooperativity between the N- and C-terminal inhibitory regions suggested that these two parts of Ets-1 may be structurally coupled. To investigate this possibility, we first performed partial proteolysis on Ets-1 to identify structural elements involved in inhibition. Digestion of Ets-1 with various amounts of trypsin generated five major tryptic peptides, designated T1 through T5 (Fig. 3A, left). A digestion time course with a single trypsin concentration gave a similar pattern (data not shown). N-terminal sequencing mapped the N termini of tryptic peptides (Fig. 3B). A native Ets-1 C terminus was identified in T3, T4, and T5 by reactivity with a C-terminus-specific antiserum (Fig. 3A, right). The total mass of protein present in each lane was essentially equal to the input protein, as determined by densitometry of the Coomassie blue-stained gels (Fig. 3A; compare lanes 2 through 7 with lane 1; densitometry data not shown). These results, in agreement with DNA titration experiments, indicate that the

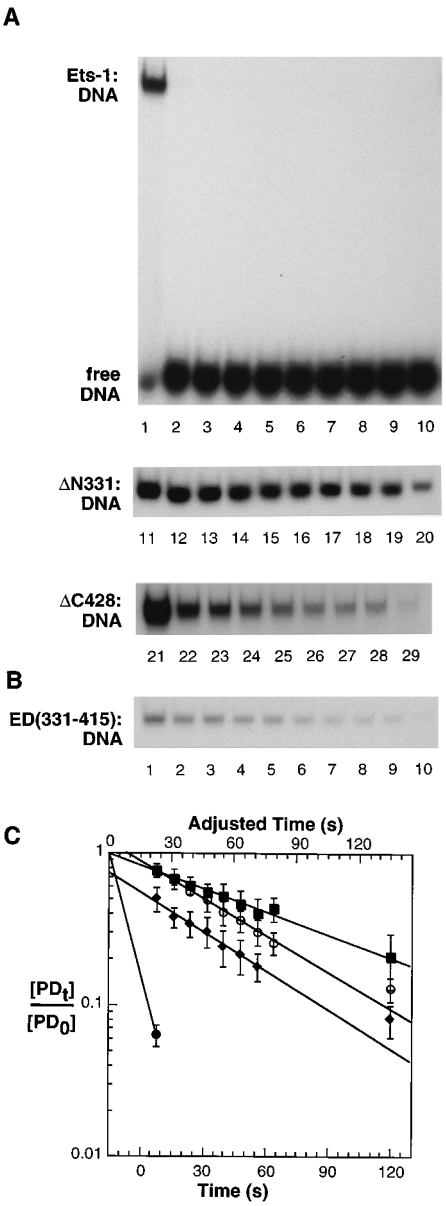

FIG. 2. Kinetic studies demonstrate a difference in the dissociation rates between Ets-1–DNA and deletion mutant-DNA complexes. (A) Dissociation of protein-DNA complexes as monitored by mobility shift assay. Reaction mixtures containing either Ets-1 (top), ΔN331 (middle), or ΔC428 (bottom) and radiolabeled SC1 DNA were allowed to reach equilibrium and challenged with unlabeled DNA, and aliquots were loaded on a mobility shift gel at timed intervals. Lanes: 1, 11, and 21, control aliquots that contained no unlabeled DNA; 2 to 9, 12 to 19, and 22 to 28, aliquots loaded at 8-s intervals; 10, 20, and 29, aliquots loaded at 120 s. For ΔN331 and ΔC428, only the portion of the autoradiogram corresponding to the protein-DNA complex is shown. (B) Dissociation of ED(331-415)-DNA complexes as monitored by mobility shift assay. Lanes: 1, control aliquot that contained no unlabeled DNA; 2 to 9, aliquots loaded at 8-s intervals; 10, aliquot loaded at 120 s. (C) Exponential decay of Ets-1–DNA (filled circle), ΔN331-DNA (squares), ΔC428-DNA (diamonds), and ED(331-415)-DNA (open circles) complexes. $[PD_t]/[PD_0]$ was measured as described in Materials and Methods. The upper time axis includes an adjustment of 15 s (see text). Data were means (± standard deviation) from two or more trials, plotted as $\log_{10}[PD_t]/[PD_0]$ versus time. Curve fits were derived from least-squares analysis of the data fitted to the equation $\ln[PD_t]/[PD_0] = -k_{-1}\,t$.

majority of Ets-1 molecules are well folded, with discrete structural domains.

The three tryptic polypeptides that contain an intact ETS domain facilitated mapping of the N-terminal inhibitory region. T3, T4, and T5 were purified from polyacrylamide gels, renatured, and used in dissociation rate experiments (Fig. 3C). The larger fragments, T3 (residues 244 to 440) and T4 (residues 280 to 440), formed DNA complexes with half-lives of less than 6 s, similar to that of full-length Ets-1. The smallest tryptic fragment, T5 (residues 310 to 440), formed a complex with a half-life similar to that of ΔN331 (half-life, 46 s; k_{-1}, 1.5×10^{-2} s^{-1}). A nondenatured mix of tryptic fragments showed the same relative dissociation rates (T3 ≅ T4 > T5; data not shown). Equilibrium binding studies on the N-terminal deletion mutant ΔN280 (residues 280 to 440) confirmed the low affinity of the T4 species (37). These mapping experiments demonstrate that the N-terminal inhibitory region can function with only 51 residues flanking the ETS domain. Thus, a relatively small fragment of Ets-1 retains inhibitory properties. T5, which is truncated by only an additional 30 residues compared with T4, displayed enhanced binding activity. Therefore, residues necessary for inhibition lie in a relatively small region between the N termini of T4 (residue 280) and T5 (residue 310). This experiment did not address whether this small region is sufficient for N-terminal inhibitory function. Indeed, as discussed below, the sequences between residues 310 and 331

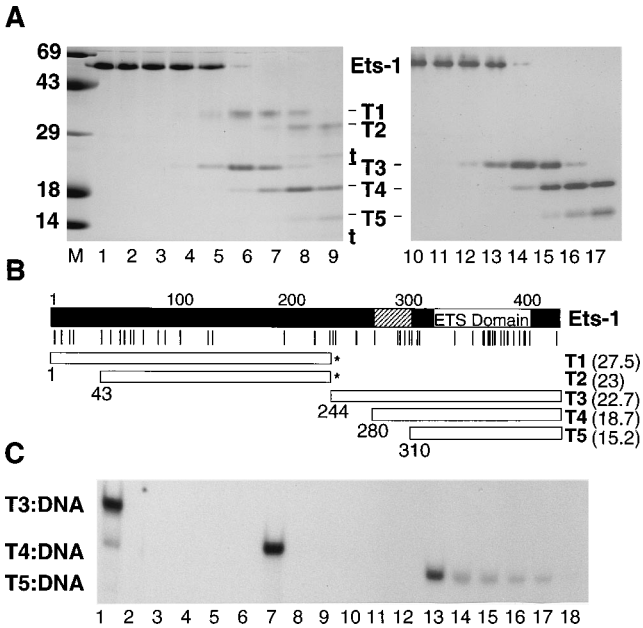

FIG. 3. Partial proteolysis of Ets-1 maps structural domains involved in inhibition. (A) Ets-1 proteolytic fragments resolved on 10 to 22% linear gradient polyacrylamide gels containing SDS. Proteins were visualized by Coomassie blue staining (left) or Western blot analysis with antibodies to the Ets-1 C terminus (right). Lanes: M, markers (molecular masses are indicated in kilodaltons); 1, mock-digested Ets-1; 2 to 9 and 10 to 17, Ets-1 incubated with 0.66, 2.0, 6.6, 20, 66, 200, 660, or 2,000 ng of trypsin per 20 μl of reaction mixture. t, trypsin or trypsin fragment. (B) Schematic representation of Ets-1 and proteolytic fragments. Vertical lines are positions of arginine and lysine residues (potential trypsin cleavage sites). Hatched areas indicate residues determined by mapping with trypsin to be necessary for inhibition. Because the decrease in Ets-1 was closely matched by the increase in T1 plus T3 (A, lanes 5 and 6), we concluded that cleavage of Ets-1 after residue 243 gave rise to these two fragments. Asterisks mark these predicted C termini. Numbers in parentheses are molecular masses in kilodaltons calculated from deduced amino acid content and agree well with size predictions from relative mobility for T3, T4, and T5. The size discrepancy for T1 and T2 may be due to aberrant mobility rather than an incorrect placement of the C termini. (C) Dissociation of tryptic fragment-DNA complexes monitored by mobility shift assay (see Fig. 2). Lanes: 1 to 6, T3-DNA; 7 to 12, T4-DNA; 13 to 18, T5-DNA; 1, 7, and 13, control aliquots that contained no unlabeled DNA; 2 to 5, 8 to 11, and 14 to 17, aliquots loaded at 8-s intervals; 6, 12, and 18, aliquots loaded at 120 s.

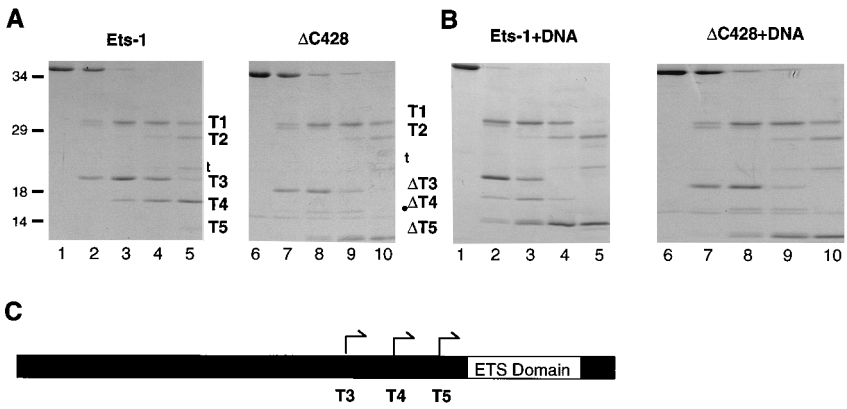

FIG. 4. Trypsin cleavage of ΔC428 and Ets-1 in the presence of DNA detects an altered conformation of the N-terminal inhibitory region. Trypsin cleavage was performed as described for Fig. 3. For trypsin cleavage in the presence of DNA, proteins were incubated with SC1 DNA (~5 μM) under standard conditions for 15 min prior to trypsin addition. Under these conditions, greater than 95% of the protein is bound to DNA. Lanes: 1 and 6, mock-digested protein; 2 to 5 and 7 to 10, Ets-1 protein incubated with 20, 66, 200, and 660 ng of trypsin per 20 μl of reaction mixture. t, trypsin band; ●, a non-DNA-binding contaminant in the ΔC428 preparation. Tryptic fragments T1 to T5 and ΔT3 to ΔT5 are labeled to the right of each gel; sizes of molecular mass standards in kilodaltons are indicated at the left. (A) Tryptic pattern produced by digestion of Ets-1 (left) and ΔC428 (right); (B) tryptic pattern produced by digestion of Ets-1 (left) and ΔC428 (right) in the presence of DNA; (C) schematic of full-length Ets-1 showing the positions of trypsin sites at codons 244 (T3), 280 (T4), and 310 (T5).

as well as portions of the ETS domain are likely to be involved in inhibition.

Previous mapping studies suggest large regions of the N terminus of Ets-1 as being necessary for inhibition (Fig. 1A) (8, 33, 49). Several studies implicate residues 244 through 328, which span the entire exon VII and include sequences present in T3, T4, and T5 (Fig. 1A). Our findings indicate that only a small region of exon VII, at most residues 280 to 328, is critical for inhibition.

Partial proteolysis provided important tools for further structural investigations of the inhibition mechanism. The protease sites at residues 280 and 310 map within the N-terminal inhibitory region and provide an assay for conformational change in this region of Ets-1. Because these sites are present in both the truncation mutant ΔC428 and full-length Ets-1, partial proteolysis could be used to monitor the structure of the N-terminal inhibitory region in high- and low-affinity forms of Ets-1. These experiments provided the key finding that structural changes in the N-terminal inhibitory region accompany derepression. Figure 4 shows the protease digestion patterns of ΔC428 and Ets-1. Tryptic fragments of ΔC428 that differ in the C termini from those of Ets-1 are distinguished by the prefix Δ. There was no difference in the patterns of appearance of tryptic fragments T1 and T2 upon digestion of Ets-1 and ΔC428. In contrast, the pattern of appearance of ΔC428 DNA-binding fragments, ΔT3 through ΔT5, differed significantly from the pattern of Ets-1 fragments T3 through T5 (Fig. 4A). In the digestion of Ets-1, T3 and T4 were the predominant proteolytic products (Fig. 4A, left). On the other hand, digestion of ΔC428 produced ΔT4 as a minor product and ΔT5 as a major product (Fig. 4A, right). Importantly, these differences mapped to the N-terminal inhibitory region. Therefore, removal of the C-terminal inhibitory region affects the protease sensitivity of the N-terminal inhibitory region. Thus, the loss of inhibition in ΔC428 is accompanied by a structural rearrangement in the N-terminal inhibitory region. We propose that this altered sensitivity is due to the loss of interaction between the N- and C-terminal inhibitory regions. This interpretation implies that the derepressed ΔC428 has lost structural, as well as functional, coupling of the two inhibitory regions.

Previous studies of the viral form of Ets-1, v-Ets, suggest that this protein is also in an altered conformation relative to the cellular protein (50). v-Ets, which is transduced by the virus E26, carries mutations in all 12 C-terminal residues (Fig. 1A) as well as a point mutation in the ETS domain (17, 30, 35, 45). We speculate that the conformational change reported for v-Ets is the same as that identified in our protease studies of ΔC428. Thus, mutation of the C terminus may be sufficient to alter the conformation of v-Ets.

Partial proteolysis of Ets-1 in the presence of DNA implicates a conformational change. We next used partial proteolysis to test for conditions in which the altered conformation of the mutant ΔC428 could be identified in full-length Ets-1. In these experiments, the conformation of Ets-1 was probed in the presence and absence of DNA. No difference was detected in tryptic fragments T1 and T2; however, T3 through T5 appeared in an altered pattern (compare Fig. 4A, left, and 4B, left). In the digestion of Ets-1 without DNA, T3 and T4 were major products, while T5 was a minor product. In contrast, digestion of Ets-1 in the presence of DNA produced T4 as a minor species and T5 as a major product. This difference in protease sensitivity suggests that a structural change in the N-terminal inhibitory region of Ets-1 occurs upon DNA binding. Importantly, the digestion pattern of Ets-1 in complex with DNA was similar to that of derepressed ΔC428 (compare Fig. 4A, right, and 4B, left). The altered conformation of ΔC428 was due to the loss of the C-terminal inhibitory region. However, both inhibitory regions are present in the full-length protein. Thus, in the case of Ets-1, conformational change of the N-terminal inhibitory region must be due to uncoupling of the interacting regions. We conclude that the N-terminal inhibitory region displays a derepressed conformation upon DNA binding. However, because Ets-1–DNA complexes dissociate rapidly and have low affinity, this uncoupled, derepressed state must be transient. In contrast, the protease sensitivity of ΔC428 was unaltered by the addition of DNA (Fig. 4B, right). Thus, the N-terminal inhibitory region of this activated mutant is always uncoupled, and ΔC428 constitutively displays the derepressed conformation.

Three important features of Ets-1 autoinhibition were detected by our protease experiments. First, the two inhibitory regions are structurally, as well as functionally, coupled. Second, derepression, caused by deletion of the C-terminal inhib-

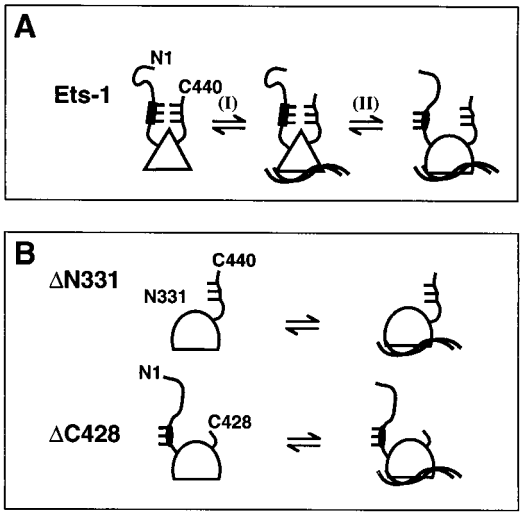

FIG. 5. Model of Ets-1 intramolecular inhibition. (A) Full-length Ets-1 with two alternative conformation states. Step I, the two inhibitory regions interact and allosterically stress the ETS domain (triangle); step II, DNA binding is accompanied by uncoupling of the two inhibitory regions. Disruption of the intramolecular interaction is characterized by a structural rearrangement (solid rectangle to oval) in the N-terminal inhibitory region. This altered conformation allosterically relaxes the ETS domain (semicircle) and transiently relieves inhibition. Reestablishment of the interaction between the two inhibitory regions causes rapid dissociation of the protein-DNA complex. (B) Ets-1 deletion mutants with one of the two inhibitory regions missing. No cooperative interactions occur between the N- and C-terminal regions of these truncations. Thus, these deletion mutants constitutively display a relaxed ETS domain and high-affinity DNA binding.

itory region, is accompanied by an altered conformation in the N-terminal inhibitory region. Finally, an identical conformational change takes place in the N-terminal inhibitory region of Ets-1 bound to DNA. In sum, these results demonstrate that conformational change plays a critical role in the mechanism of inhibition.

DISCUSSION

A mechanistic model of Ets-1 autoinhibition. Figure 5 presents our mechanistic model for autoinhibition of Ets-1 DNA binding. Full-length Ets-1, with two intact inhibitory regions, provides the most complete picture (Fig. 5A). In the first step of the model, the two inhibitory regions interact and maintain the ETS domain in a stressed conformation (triangular ETS domain). In the second step of the model, DNA binding disrupts the interaction between the two inhibitory regions. Loss of structural coupling between the two inhibitory regions leads to an altered conformation within the N-terminal inhibitory region (rectangle to oval) and allows the ETS domain to relax. A relaxed ETS domain (depicted as a semicircle) makes more stable contact with DNA. However, this relaxed conformation is transient. Reestablishment of the interaction between inhibitory regions returns the ETS domain to the stressed conformation and causes rapid dissociation from DNA. Deletion of either inhibitory region prevents the intramolecular interactions between the two inhibitory regions, thus allowing a constitutively relaxed, derepressed state (Fig. 5B). This model is supported by the functional and structural data discussed below.

Interaction between inhibitory regions is cooperative. A cooperative interaction between the two inhibitory regions is supported by several pieces of data. Kinetic experiments demonstrated that both regions function by enhancing dissociation of the protein-DNA complex. In addition, neither region acted independently of the other; the presence of a single inhibitory region did not mediate inhibition. Furthermore, a mutant lacking both inhibitory regions showed no greater activation than either singly deleted form. Taken together, these observations establish that the two inhibitory regions act cooperatively through a common pathway.

A cooperative model of Ets-1 inhibition has been previously proposed on the basis of studies of N- and C-terminal deletion mutants and a v-Ets construct that is mutated in the C-terminal inhibitory region (22, 33, 49). However, none of the previous studies analyzed both N- and C-terminal deletion mutants to obtain accurate binding affinities. Importantly, the DNA-binding activity of the minimal ETS domain, from which both inhibitory regions are deleted, has not been previously reported. Thus, the data presented here are the first conclusive biochemical evidence for cooperative coupling between two separate inhibitory regions.

Our analyses also provide unique structural data that support a cooperative model. Partial proteolysis of ΔC428 detected altered protease sensitivity within the N-terminal inhibitory region. This result demonstrated that removal of the C-terminal inhibitory region affected the structure of the N-terminal inhibitory region. Thus, we propose that loss of inhibition is due to loss of coupling between the two inhibitory regions.

An allosteric mechanism regulates DNA-binding affinity. In contrast to previous models of Ets-1 DNA binding in which the inhibitory region sterically masks the DNA-binding surface (33), our data suggest that an allosteric mechanism regulates Ets-1 DNA binding. If inhibition of Ets-1 were due to a masking of the ETS domain that required a kinetically slow opening step, association rates of repressed and activated forms would differ greatly. The calculated association rate constants of repressed Ets-1 and activated ΔC428 were very similar; however, the dissociation rates differed by as much as 10-fold. Thus, our results demonstrate that the majority of difference in DNA-binding affinity is due to a difference in dissociation rates rather than association rates. These results strongly suggest that Ets-1 DNA binding is not regulated through a steric masking of the ETS domain. These findings have led to a new mechanistic model of Ets-1 autoinhibition. We propose that the inhibitory regions allosterically stress the ETS domain and destabilize DNA contacts.

An altered conformation accompanies derepression and DNA binding. The altered conformation of Ets-1 is key to understanding the mechanism of inhibition. Two partial proteolysis experiments detected conformational changes in Ets-1 polypeptides. First, the high-affinity mutant ΔC428 displayed an altered protease sensitivity in the N-terminal inhibitory region. These findings indicated that deletion of the C-terminal inhibitory region not only derepressed DNA-binding activity but also caused a change in conformation of the N-terminal inhibitory region. Next, partial proteolysis detected this identical conformation in full-length Ets-1 bound to DNA; the derepressed conformation observed with high-affinity ΔC428 is revealed during Ets-1 DNA binding. This result suggested that the inhibitory regions of Ets-1 uncouple upon DNA binding. However, because both inhibitory regions are intact, reestablishment of the interaction leads to dissociation from DNA. In sum, the structural uncoupling of the inhibitory regions is critical for modulating DNA binding of both high- and low-affinity Ets-1 polypeptides.

Structural studies support an allosteric, cooperative model. Recent NMR studies of ETS domain proteins support the

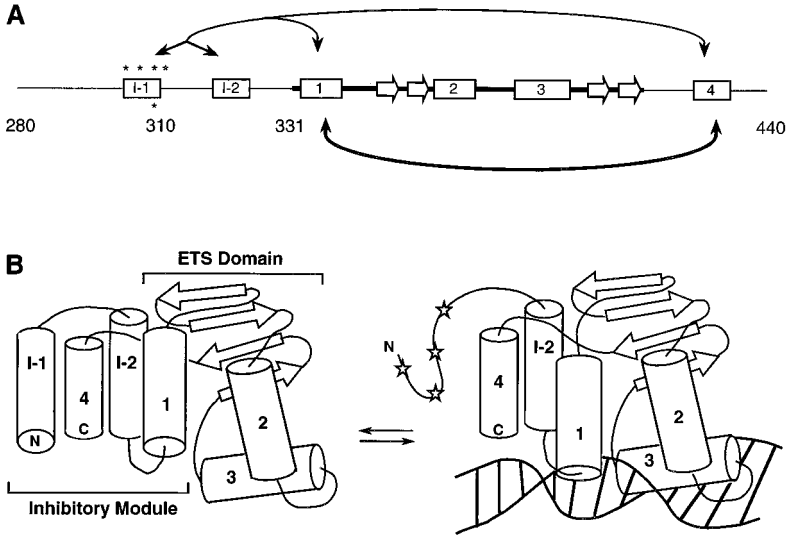

FIG. 6. Structural data and modeling of the Ets-1 inhibitory module. (A) Summary of structural studies of the ETS domain and inhibitory module of Ets-1. Coordinates refer to residue numbers in full-length Ets-1. Positions 331 to 415 are within the ETS domain. The secondary structure of the ETS domain is based on NMR experiments (4, 5, 43, 51). Rectangles and arrows on gene structure represent α-helices and β-strands, respectively. Bold line connections represent NMR data, including nuclear Overhauser effect-based connectivity from the solution structure of the high-affinity species ΔN331 (5). Light line connections represent NMR connectivity derived from changes in chemical shifts of specific residues between 331 to 440 in the presence and absence of the N-terminal inhibitory region (43). Asterisks mark protease-sensitive sites mapped in either ΔN280 (37) (above the line) or Ets-1 (below the line). (B) Proposed three-dimensional model of the inhibitory module in the presence and absence of DNA. This schematic picture accommodates all known secondary structure elements within the ΔN280 fragment and the established three-dimensional structure of the ETS domain with the C-terminal inhibitory helix (4, 5, 51). The unstructured region amino terminal to the first inhibitory helix has not been included. The positioning of the two helices of the N-terminal inhibitory region is based on NMR chemical shift data (43) and the structural coupling data presented in this report. The first α-helix in the N-terminal inhibitory region is induced to unfold in the presence of DNA (37). Asterisks mark the locations of protease cleavage sites exposed upon DNA binding. As discussed in the text, the structure of the ETS domain in the presence of DNA is derived from the studies of high-affinity species (51). The difference in position of the first helix of the ETS domain in the left and right panels reflects one possible structural change that could accompany the proposed (stressed to relaxed) transition of the DNA-binding motif upon DNA binding.

model proposed here (summarized in Fig. 6). NMR-based structures of Ets-1 and Fli-1 show that the ETS domain contains three α-helices and a four-stranded β-sheet (4, 5, 31, 51). The second and third α-helices form a helix-turn-helix DNA-binding motif that binds in the major groove of the DNA. The amino terminus of the first α-helix binds the minor groove by a novel mechanism that involves intercalation of a single tryptophan residue (51). Although the three-dimensional structural study of Ets-1–DNA complexes was performed on only a high-affinity *ets-1* fragment (51), biochemical and genetic studies indicate that low-affinity fragments will display this same DNA-protein interface. DNase I protection, alkylation interference patterns, and binding-site selection data are similar between the full-length and truncated Ets-1 polypeptides (9, 36, 53). A DNase I-hypersensitive site that accompanies ETS domain DNA binding is particularly informative. This hypersensitive site is likely due to the altered DNA conformation that accompanies the tryptophan intercalation and minor groove binding. The invariant appearance of this site in both low- and high-affinity Ets-1–DNA complexes strongly suggests that low-affinity species will mediate the combination of major and minor groove interactions reported for the high-affinity species.

NMR studies of the high-affinity species ΔN331 identified an additional α-helix in the C-terminal inhibitory region and demonstrated by nuclear Overhauser effect spectroscopy experiments a direct structural connection between this helix and the first helix of the ETS domain (4, 5). NMR analyses of the low-affinity species ΔN280 identified two α-helices within the N-terminal inhibitory region. The presence of these two α-helices significantly alters the chemical shifts within the first α-helix of the ETS domain and the C-terminal α-helix (43). These NMR data indicate that the N-terminal inhibitory region is structurally coupled to the C-terminal inhibitory region and the ETS domain. These findings provide strong support for our cooperative model in which the two inhibitory regions are both structurally and functionally linked. The results are in good agreement with our protease studies which indicated that the two inhibitory regions are structurally coupled. Additionally, the NMR experiments demonstrated that the C-terminal inhibitory region, and possibly the N-terminal inhibitory region, directly contacts the ETS domain. The direct interaction of the inhibitory regions with the ETS domain provides a structural connection that is consistent with the allosteric feature of our model.

DNA binding studies of ΔN331 and ΔN280 support our analyses of full-length Ets-1. The difference in binding affinity, K_D, between ΔN280 and ΔN331 is ~15-fold (37), while the difference between Ets-1 and ΔN331 is ~23-fold. This comparison suggests that ΔN280 and full-length Ets-1 display approximately the same inhibitory potentials. Thus, the autoinhibition mechanism is fully functional within the ΔN280 fragment, and the structural elements contained in ΔN280 can be used to model inhibition of full-length Ets-1.

Biophysical studies of ΔN331 and ΔN280 indicate that the first α-helix in the amino-terminal inhibitory region unfolds upon DNA binding (Fig. 6) (37). The protease and kinetics experiments reported here integrate this finding into our proposed mechanism of Ets-1 DNA binding. This structural rearrangement was detected in part by protease probing. The protease susceptibility of residues between 304 and 312 in ΔN280 is consistent with the hypersensitivity of residue 310 in Ets-1. In both proteins, cleavage is enhanced in the presence of DNA. These results strongly suggest that the α-helix in the amino-

terminal inhibitory region in full-length Ets-1 also unfolds upon DNA binding. We have proposed that unfolding of this helix disrupts the cooperative interactions of the inhibitory regions and thus allows the ETS domain to bind DNA. Kinetic studies describe short half-lives for both Ets-1- and ΔN280-DNA complexes. Taken together, these data indicate that the reestablishment of the inhibitory interactions leads to rapid dissociation of Ets-1 from DNA. Furthermore, this event is likely to involve refolding of the inhibitory α-helix.

The findings of these structural studies combined with the data presented here lead to a more detailed version of our cooperative, allosteric model of autoinhibition (Fig. 6B). In the absence of DNA, an intact inhibitory module contains three inhibitory helices and the first helix of the ETS domain packed into a bundle-like structure (Fig. 6B, left). In this three-dimensional arrangement, direct structural coupling of the N- and C-inhibitory regions explains the functional cooperation of these two regions. This picture also accommodates the allosteric mechanism of inhibition. The first helix of the ETS domain packs against helices of both inhibitory regions as well as the helix-turn-helix motif. Thus, this helix couples the N- and C-inhibitory regions to the DNA binding domain of Ets-1. In the presence of DNA, the inhibitory module is disrupted, which leads to a loss in the cooperative interactions between the two inhibitory regions (Fig. 6B, right). This structural rearrangement is most dramatically evidenced by the unfolding of the N-terminal inhibitory helix. As indicated by the kinetic studies, the reestablishment of the inhibitory module, including the refolding of the inhibitory helix, leads to rapid dissociation of Ets-1 from DNA.

Proposed biological modulation of inhibition. These data demonstrate that the ETS domain within the full-length Ets-1 polypeptide has the potential to bind DNA with high affinity. A variety of regulatory events could uncover the full DNA-binding potential of the ETS domain: proteolysis, association with other proteins, or posttranslational modifications. In our structural model of Ets-1 DNA binding, a partner protein could relieve inhibition by stabilizing the relaxed conformation. In support of this hypothesis, Ets-1 functions in collaboration with a variety of other transcription factors. Ets-1 synergizes with Sp1 in activating transcription from the human T-cell lymphotropic virus type 1 enhancer (13). Myb, which is transduced along with Ets by the virus E26, has also been shown to cooperate with Ets-1 at the *mim* promoter and a myeloid cell-specific promoter (6, 41). Ets-1 works with a Jun-Fos heterodimer on the polyomavirus enhancer (48), while it cooperates with PU.1 on the immunoglobulin μ-chain enhancer (34). Most recently, Ets-1 has been shown to work with the core-binding factor (CBF/PEBP2) on several viral and cellular enhancers, including those of the T-cell receptor α and β subunit genes (14, 46, 54). Furthermore, DNA binding cooperativity has been demonstrated in the case of the core-binding factor and Ets-1 (14, 36a, 54).

Partner proteins also have been shown to regulate DNA binding of other *ets* family members. In the case of Ets proteins that interact with the serum response factor, sequences outside the ETS domain mediate the cooperative interaction (2, 16). The α subunit of the ETS domain protein GA-binding protein (GABP) provides another relevant example. Addition of the GABP β subunit to the α subunit increases the half-life of the DNA-GABP complex (47). Thus, modulating dissociation may be a general method of regulating the DNA binding of Ets proteins.

Inhibition also could be modulated by phosphorylation since Ets-1 is a phosphoprotein (10, 38, 39). An analysis of the in vivo phosphorylation of Ets-1 indicates that four sites lie within the T3 fragment, while two are retained in the T4 fragment (39). Phosphorylation could favor either the stressed or relaxed conformation.

Our findings support a model in which an inhibitory module, composed of two separate regions, allosterically modulates the DNA-binding activity of Ets-1. Autoinhibition has been observed in a variety of other proteins, including kinases and phosphatases (7, 27, 44). As in the case of Ets-1, activation of these enzymes requires conformational rearrangements. On a more general level, allosteric effects and conformational change are well-characterized ways to regulate protein function. Our work contributes to the growing appreciation that these processes are utilized by transcription factors to execute a variety of functions.

ACKNOWLEDGMENTS

We thank D. Goldenberg, L. McIntosh, D. Stillman, and D. Virshup for critical reading of the manuscript and R. Schackmann for protein sequencing.

This work was funded by the National Institutes of Health (grants GM38663 to B.J.G. and CA42014 to the Huntsman Cancer Institute for core facility support).

REFERENCES

1. **Carey, J.** 1991. Gel retardation. Methods Enzymol. **208:**103–117.
2. **Dalton, S., and R. Treisman.** 1992. Characterization of SAP-1, a protein recruited by serum response factor to the c-*fos* serum response element. Cell **68:**597–612.
3. **Doering, D. S.** 1992. Ph.D. thesis. Massachusetts Institute of Technology, Cambridge, Mass.
4. **Donaldson, L. W., J. M. Petersen, B. J. Graves, and L. P. McIntosh.** 1994. Secondary structure of the ETS domain places murine Ets-1 in the superfamily of winged helix-turn-helix DNA-binding proteins. Biochemistry **33:** 13509–13516.
5. **Donaldson, L. W., J. M. Petersen, B. J. Graves, and L. P. McIntosh.** 1996. Solution structure of the ETS domain from murine Ets-1: a winged helix-turn-helix DNA binding motif. EMBO J. **15:**125–134.
6. **Dudek, H., R. V. Tantravahi, V. N. Rao, E. S. P. Reddy, and E. P. Reddy.** 1992. Myb and Ets proteins cooperate in transcriptional activation of the *mim-1* promoter. Proc. Natl. Acad. Sci. USA **89:**1291–1295.
7. **Erpel, T., G. Superti-Furga, and S. Courtneidge.** 1995. Mutational analysis of the Src SH3 domain: the same residues of the ligand binding surface are important for intra- and intermolecular interactions. EMBO J. **14:**963–975.
8. **Fisher, R. J., M. Favash, J. Casas-Finet, J. W. Erickson, A. Kondoh, S. V. Bladen, C. Fisher, D. K. Watson, and T. Papas.** 1994. Real-time DNA binding measurements of the ETS1 recombinant oncoproteins reveal significant kinetic differences between the p42 and p51 isoforms. Protein Sci. **3:**257–266.
9. **Fisher, R. J., G. Mavrothalassitis, A. Kondoh, and T. S. Papas.** 1991. High-affinity DNA-protein interactions of the cellular ETS1 protein: the determination of the ETS binding motif. Oncogene **6:**2249–2254.
10. **Fleischman, L. F., A. M. Pilaro, K. Murakami, A. Kondoh, R. J. Fisher, and T. S. Papas.** 1993. c-Ets-1 protein is hyperphosphorylated during mitosis. Oncogene **8:**771–780.
11. **Frankel, A. D., and P. S. Kim.** 1991. Modular structure of transcription factors: implications for gene regulation. Cell **65:**717–719.
12. **Fried, M. G.** 1989. Measurement of protein-DNA interaction parameters by electrophoresis mobility shift assay. Electrophoresis **10:**366–376.
13. **Gegonne, A., R. Bosselut, R. Bailly, and J. Ghysdael.** 1993. Synergistic activation of the HTLV1 LTR Ets-responsive region by transcription factors Ets1 and Sp1. EMBO J. **12:**1169–1178.
14. **Giese, K., C. Kingsley, J. R. Kirshner, and R. Grosschedl.** 1995. Assembly and function of a TCRα enhancer complex is dependent on LEF-1 induced DNA bending and multiple protein-protein interactions. Genes Dev. **9:**995–1008.
15. **Gill, S. C., and P. H. von Hippel.** 1989. Calculation of protein extinction coefficients from amino acid sequence data. Anal. Biochem. **182:**319–326.
16. **Giovane, A., A. Pintzas, S. Maira, P. Sobieszczuk, and B. Wasylyk.** 1994. Net, a new *ets* transcription factor that is activated by Ras. Genes Dev. **8:**1502–1513.
17. **Golay, J., M. Introna, and T. Graf.** 1988. A single point mutation in the v-ets oncogene affects both erythroid and myelomonocytic cell differentiation. Cell **55:**1147–1158.
18. **Green, M., T. J. Schuetz, E. K. Sullivan, and R. E. Kingston.** 1995. A heat shock-responsive domain of human HSF that regulates transcription activation domain function. Mol. Cell. Biol. **15:**3354–3362.

19. **Grimm, S., and P. A. Baeuerle.** 1993. The inducible transcription factor NF-kappa B: structure-function relationship of its protein subunits. Biochem. J. **290:**297–308.
20. **Gunther, C. V., and B. J. Graves.** 1994. Identification of ETS domain proteins in murine T lymphocytes that interact with the Moloney murine leukemia virus enhancer. Mol. Cell. Biol. **14:**7569–7580.
21. **Hager, D. A., and R. R. Burgess.** 1980. Elution of proteins from sodium dodecyl sulfate, and renaturation of enzymatic activity: results with sigma subunit of E. coli RNA polymerase, wheat germ DNA topoisomerase, and other enzymes. Anal. Biochem. **109:**76–86.
22. **Hagman, J., and R. Grosschedl.** 1992. An inhibitory carboxyl terminal domain in Ets-1 and Ets-2 mediates differential binding of ETS family factors to promoter sequences of the *mb-1* gene. Proc. Natl. Acad. Sci. USA **89:** 8889–8893.
23. **Hahn, S. L., and B. Wasylyk.** 1994. The oncoprotein v-Ets is less selective in DNA binding than c-Ets-1 due to the C-terminal sequence change. Oncogene **9:**2499–2512.
24. **Harlow, E., and D. Lane.** 1988. Antibodies: a laboratory manual. Cold Spring Harbor Laboratory, Cold Spring Harbor, N.Y.
25. **Hupp, T. R., D. W. Meek, C. A. Midgley, and D. P. Lane.** 1992. Regulation of the specific DNA binding function of p53. Cell **71:**875–886.
26. **Hupp, T. R., A. Sparks, and D. P. Lane.** 1995. Small peptides activate the latent sequence-specific DNA binding function of p53. Cell **83:**237–245.
27. **Kemp, B. E., and R. B. Pearson.** 1991. Intrasteric regulation of protein kinases and phosphatases. Biochim. Biophys. Acta **1094:**67–76.
28. **Kowenz-Leutz, E., G. Twamley, S. Ansieau, and A. Leutz.** 1994. Novel mechanism of C/EBP (NF-M) transcriptional control: activation through derepression. Genes Dev. **8:**2781–2791.
29. **Laemmli, U. K.** 1970. Cleavage of structural proteins during the assembly of the head of bacteriophage T4. Nature (London) **227:**680–685.
30. **Leprince, D., A. Gegonne, J. Coll, C. de Taisne, A. Schneeberger, C. Lagrou, and D. Stehelin.** 1983. A putative second cell-derived oncogene of the avian leukaemia retrovirus E26. Nature (London) **306:**395–397.
31. **Liang, H., X. Mao, E. Olenjniczak, D. G. Nettesheim, L. Yu, R. P. Meadows, C. B. Thompson, and S. W. Fesik.** 1994. Solution structure of the *ets* domain of Fli-1 when bound to DNA. Nat. Struct. Biol. **1:**871–876.
32. **Lieberman, P. M., M. C. Schmidt, C. C. Kao, and A. J. Berk.** 1991. Two distinct domains in the yeast transcription factor IID and evidence for a TATA box-induced conformational change. Mol. Cell. Biol. **11:**63–74.
33. **Lim, F., N. Kraut, J. Frampton, and T. Graf.** 1992. DNA binding by c-Ets-1, but not v-Ets, is repressed by an intramolecular mechanism. EMBO J. **11:**643–652.
34. **Nelsen, B., T. Gang, B. Erman, J. Gregoire, R. Maki, B. Graves, and R. Sen.** 1993. Regulation of lymphoid-specific immunoglobulin μ heavy chain gene enhancer by ETS-domain proteins. Science **261:**82–86.
35. **Nunn, M. F., P. H. Seeburg, C. Moscovici, and P. H. Duesberg.** 1983. Tripartite structure of the avian erythroblastosis virus E26 transforming gene. Nature (London) **306:**391–395.
36. **Nye, J. A., J. M. Petersen, C. V. Gunther, M. D. Jonsen, and B. J. Graves.** 1992. Interaction of murine Ets-1 with GGA-binding sites establishes the ETS domain as a new DNA-binding motif. Genes Dev. **6:**975–990.

36a. **Petersen, J., T. Gu, N. Speck, and B. Graves.** Unpublished data.

37. **Petersen, J. M., J. J. Skalicky, L. W. Donaldson, L. P. McIntosh, T. Alber, and B. J. Graves.** 1995. Modulation of transcription factor Ets-1 DNA binding: DNA-induced unfolding of an alpha helix. Science **269:**1866–1869.
38. **Pognonec, P., K. E. Boulukos, J. C. Gesquiere, D. Stehelin, and J. Ghysdael.** 1988. Mitogenic stimulation of thymocytes results in the calcium-dependent phosphorylation of c-*ets*-1 proteins. EMBO J. **7:**977–983.
39. **Rabault, B., and J. Ghysdael.** 1994. Calcium-induced phosphorylation of ETS1 inhibits its specific DNA binding activity. J. Biol. Chem. **269:**28143–28151.
40. **Rabindran, S. K., R. I. Haroun, J. Clos, J. Wisniewski, and C. Wu.** 1993. Regulation of heat shock factor trimer formation: role of a conserved leucine zipper. Science **259:**230–234.
41. **Shapiro, L. H.** 1995. Myb and Ets proteins cooperate to transactivate an early myeloid gene. J. Biol. Chem. **270:**8763–8771.
42. **Shi, Y., P. E. Kroeger, and R. I. Morimoto.** 1995. The carboxyl-terminal transactivation domain of heat shock factor 1 is negatively regulated and stress responsive. Mol. Cell. Biol. **15:**4309–4318.
43. **Skalicky, J. J., L. W. Donaldson, J. M. Petersen, B. J. Graves, and L. P. McIntosh.** 1996. Structural coupling of the inhibitory regions flanking the ETS domain of murine Ets-1. Protein Sci. **5:**296–309.
44. **Soderling, T. R.** 1990. Protein kinases: regulation by auto-inhibitory domains. J. Biol. Chem. **265:**1823–1826.
45. **Soudant, J., O. Albabli, P. Dhordain, A. Flourens, D. Stehelin, and D. Leprince.** 1994. A residue of the ETS domain mutated in the v-ets oncogene is essential for the DNA-binding and transactivating properties of the ETS-1 and ETS-2 proteins. Nucleic Acids Res. **22:**3871–3879.
46. **Sun, W., B. J. Graves, and N. A. Speck.** 1995. Transactivation of the Moloney murine leukemia virus and T-cell receptor β-chain enhancers by *cbf* and *ets* requires intact binding sites for both proteins. J. Virol. **69:**4941–4949.
47. **Thompson, C. C., T. A. Brown, and S. L. McKnight.** 1991. Convergence of Ets- and Notch-related structural motifs in a heteromeric DNA binding complex. Science **253:**762–768.
48. **Wasylyk, C., P. Flores, A. Gutman, and B. Wasylyk.** 1989. PEA3 is a nuclear target for transcription activation by non-nuclear oncogenes. EMBO J. **8:**3371–3378.
49. **Wasylyk, C., J.-P. Kerckaert, and B. Wasylyk.** 1992. A novel modulator domain of Ets transcription factors. Genes Dev. **6:**965–974.
50. **Wasylyk, C., and B. Wasylyk.** 1993. Oncogenic conversion of Ets affects redox regulation in-vivo and in-vitro. Nucleic Acids Res. **21:**523–529.
51. **Werner, M. H., G. M. Clore, C. L. Fisher, R. J. Fisher, L. Tring, J. Shiloach, and A. M. Cronenborn.** 1995. The solution structure of the human ETS1-DNA complex reveals a novel mode of binding and true side chain intercalation. Cell **83:**761–771.
52. **Williams, S. C., M. Baer, A. J. Dillner, and P. F. Johnson.** 1995. CRP(C/EBPβ) contains a bipartite regulatory domain that controls transcriptional activation, DNA binding and cell specificity. EMBO J. **14:**3170–3183.
53. **Woods, D. B., J. Ghysdael, and M. J. Owen.** 1992. Identification of nucleotide preferences in DNA sequence recognized specifically by c-Ets-1 protein. Nucleic Acids Res. **20:**699–704.
54. **Wotton, D., J. Ghysdael, S. Wang, N. A. Speck, and M. J. Owen.** 1994. Cooperative binding of Ets-1 and core binding factor to DNA. Mol. Cell. Biol. **14:**840–850.
55. **Zou, J., D. Rungger, and R. Voellmy.** 1995. Multiple layers of regulation of human heat shock transcription factor 1. Mol. Cell. Biol. **15:**4319–4330.